JACS
JOURNAL OF THE AMERICAN CHEMICAL SOCIETY
Article
Cite This: J. Am. Chem. Soc. 2019, 141, 15972−15976
pubs.acs.org/JACS

Ferroelectricity and Rashba Effect in a Two-Dimensional Dion-Jacobson Hybrid Organic−Inorganic Perovskite

In-Hyeok Park,[†] Qiannan Zhang,[‡] Ki Chang Kwon,[†] Ziyu Zhu,[†] Wei Yu,[†] Kai Leng,[†] David Giovanni,[‡] Hwa Seob Choi,[†] Ibrahim Abdelwahab,[†] Qing-Hua Xu,[†] Tze Chien Sum,*[,‡] and Kian Ping Loh*[,†]

[†]Department of Chemistry, National University of Singapore, 3 Science Drive 3, Singapore 117543, Singapore
[‡]Division of Physics and Applied Physics, School of Physical and Mathematical Sciences, Nanyang Technological University, 21 Nanyang Link, Singapore 637371, Singapore

Supporting Information

ABSTRACT: Hybrid organic−inorganic perovskites (HOIPs) are a new generation of high-performance materials for solar cells and light emitting diodes. Beyond these applications, ferroelectricity and spin-related properties of HOIPs are increasingly attracting interests. The presence of strong spin−orbit coupling, allied with symmetry breaking ensured by remanent polarization, should give rise to Rashba-type splitting of electronic bands in HOIP. However, the report of both ferroelectricity and Rashba effect in HOIP is rare. Here we report the observation of robust ferroelectricity and Rashba effect in two-dimensional Dion-Jacobson perovskites.

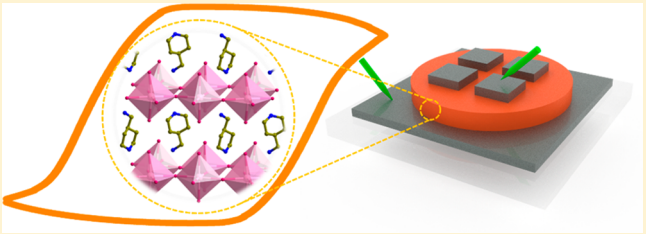

INTRODUCTION

Recently, 2D perovskites of the Ruddlesden−Popper (RP) class and its higher dimensional homologues (quasi-2D) have emerged from the shadows of 3D perovskites because of their higher chemical stability, as well as the newly discovered solar cell performance by edge oriented quasi-2D perovskites.[1,2] At the same time, there is blooming interests in the ferroelectric properties of these 2D perovskites since spontaneous polarization in ferroelectric semiconductor enhances charge separation and can potentially break the Shockley-Queisser limit through the bulk photovoltaic effect.[3−9] Room temperature ferroelectric phase has been reported in $(BA)_2(MA)_{(n-1)}Pb_nX_{(3n+1)}$-type perovskites (where BA = $C_4H_9NH_3^+$; MA = $CH_3NH_3^+$; X = Br or Cl);[10−12] tunable ferroelectricity has also been observed in RP perovskites $(PEA)_2(MA)_{(n-1)}Pb_nI_{(3n+1)}$ (where PEA = $C_6H_5C_2H_4NH_3^+$) due to correlated reorientation of MA and ion translations.[5] Molecular engineer of organic cations that introduce lattice distortion and molecular reorientation can lead to an order−disorder type transition at Curie temperature above room temperature.[13,14]

The prerequisite for ferroelectricity is the lack of centrosymmetry in the crystal, together with a strong spin−orbit coupling (SOC) ensured by the heavy Pb atoms, and these conditions give rise to the Rashba effect. The coexistence of ferroelectricity and Rashba effect gives rise to a class of spintronics-relevant material called Rashba ferroelectrics, among which includes GeTe.[15−19] In such material, the spin−orbit coupling, as well as the spin texture, is influenced by the switchable electric polarization. In the absence of structural inversion symmetry, the spin-degenerate parabolic band splits into two spin-polarized bands, where the electron (or/and hole) dispersion relation may be described by $E_{\pm}(k) = \frac{\hbar^2 k^2}{2m^*} \pm \alpha|k|$, where α_R is the Rashba splitting parameter.[19−21] A giant Rashba splitting was previously reported for $(PEA)_2PbI_4$, with energy splitting of (40 ± 5) meV and Rashba parameter of 1.6 eV·Å (Figure 1a).[19]

As an alternative to the much studied RP perovskite class (Figure 1a), Dion-Jacobson (DJ) phase HOIPs are known for

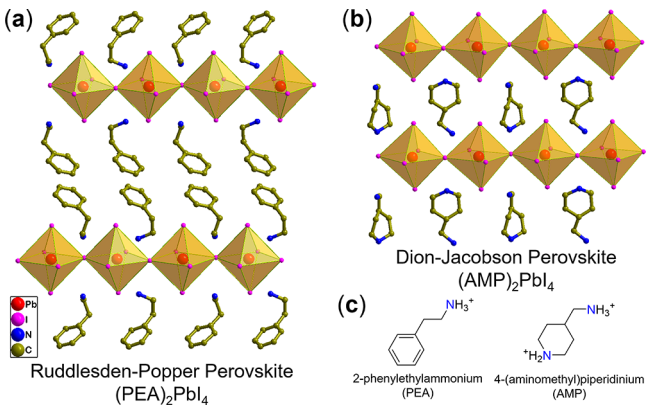

Figure 1. Structural comparison of 2D hybrid organic−inorganic (a) Ruddlesden−Popper and (b) Dion-Jacobson perovskites and (c) chemical structures of amine derivatives.

Received: July 21, 2019
Published: September 16, 2019

DOI: 10.1021/jacs.9b07776
J. Am. Chem. Soc. 2019, 141, 15972−15976

their higher stability because the van der Waals gap is replaced by diammonium cations that are hydrogen bonded to the inorganic layers on both sides (Figure 1b).[22−24] Phase change involving the reorientation of these cations may be associated with paraelectric-ferroelectric transition. In this paper, we report robust ferroelectricity and Rashba effect in 2D DJ-HOIP (Figure 1b) of the formula $(AMP)PbI_4$ (where AMP is 4-(aminomethyl)piperidinium (Figure 1c))

RESULTS AND DISCUSSION

The DJ perovskite studied here belong to n = 1 DJ perovskite, with a visible photoluminescence peaked at 523 nm and an optical band gap of ∼2.38 eV (Figure S2). Structural phase changes in $(AMP)PbI_4$ (hereafter denoted **DJP**) at 293 and 373 K were tracked using single crystal X-ray diffraction (SC-XRD) analysis. SC-XRD reveals that room-temperature phase (RTP) of **DJP** at 298 K crystallizes in the monoclinic Pc phase, which is noncentrosymmetric.[22] In RTP, the asymmetric unit contains two AMP molecules, two Pb atoms, and 8 I atoms (Figure S4a). The AMP cations (based on -NH_3) are oriented alternatively in an up and down configuration in the interlayers of $[PbI_4]^{2-}$ (Figure 2a). The Pb atoms are located in the (green-colored)

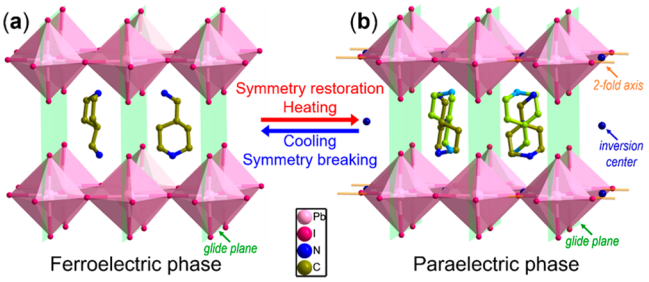

Figure 2. Symmetry restoration/breaking of single crystal structures of **DJP** in (a) ferroelectric phase at 298 K with space group Pc and (b) paraelectric phase with space group $P2_1/c$ at 373 K.

glide plane, which is the only symmetry element in **DJP**. The AMP molecules are situated below the center line dividing the inorganic layers along a-axis (Figure S6). This asymmetry facilitates polarization which is directed along the $[\bar{1}00]$ equivalent direction.

DJP crystallizes in the monoclinic phase at 373 K, corresponding to the $P2_1/c$ high temperature phase (HTP), which is centrosymmetric (Table S1). The asymmetric unit of HTP is reduced to half of that of RTP and contains one AMP molecule, one Pb atom, and 4 iodine atoms (Figure S4b). In HTP, the AMP molecules are located at the inversion center, causing the polarization to be canceled (Figure 2b and Figure S7). As depicted in Figure 2b, the HTP structure has the (green-colored) glide plane and also the (orange-colored) 2-fold axis and the (navy-colored) inversion center.

The thermal anomalies in **DJP** that accompanies the ferroelectric-paraelectric transition was confirmed by variable temperature differential scanning calorimetry (DSC) curves and second harmonic generation (SHG) signal in a heating−cooling cycle (Figure 3). A pair of thermal anomalies from DSC curve in **DJP** was observed at 352 K in the heating process and 349 K in the cooling process (Figure 3a). The DSC provides the reversible phase transition temperature at T_c = 352 K. Since SHG signal is only generated from noncentrosymmetric materials,[13] symmetry breaking by phase transition in **DJP** was

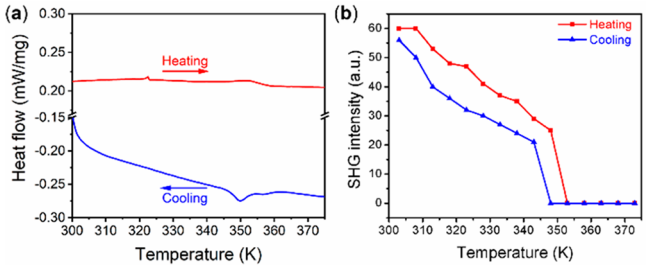

Figure 3. Temperature-dependent properties of **DJP** in a heating−cooling cycle. (a) DSC curves. (b) SHG signal intensity.

monitored by SHG measurement, from which the Curie temperature of **DJP** is T_c = 353 K (Figure 3b).

Having established the noncentrosymmetric nature of **DJP**, we next investigate if **DJP** is ferroelectric at room temperature using Piezoresponse force microscopy (PFM). Figure 4 presents images constructed by out-of-plane PFM amplitude and phase, which reveal two types of domain structures on the thin-film of **DJP**. The phase image is distinct from the topography image in Figure 4a, thus ruling out morphology as the origin for the phase contrast. The thin-film was first polarized by applying a dc bias of V = 3 V on the conductive tip with the conducting substrate (Au coated Si wafer) grounded (Figure 4b). With respect to the dc voltage polarity, the light-orange regions (Figure 4b) represent the ferroelectric domains oriented out-of-plane in the sample (and along the applied dc field direction of the tip), whereas the brown regions represent the domains with random orientations, as illustrated in Figure 4b,c. Figure 4d,e shows the remnant and amplitude hysteresis loops for **DJP** on a random sample spot. To eliminate the electrostatic interactions from the tip and sample which may originate from hysteretic surface charging, pulsed voltage with a maximum of 8 V was applied, and only the remnant signal was used for analysis in this study. The PFM amplitude hysteresis loop is shown in Figure 4e, the well-defined butterfly loops and the 180° phase switching at room temperature are indicative of ferroelectric polarization in **DJP** (Figure 4f).

The polarization switching was also checked by collecting $I-V$ and $P-V$ curves in a semiconductor analyzer. The device was fabricated using a 250 μm-thick **DJP** pellet with top and bottom Ag electrodes (Figure 5a). It has two apparent current peaks at ±10 V corresponding to the ferroelectric switching voltage (coercive voltage), indicating that the device resistance is changed by polarization switching of **DJP** (Figure 5b). As depicted in Figure 5b, the green arrows displays the voltage sweep directions (−15 V → 0 V → +15 V → 0 V → − 15 V). The **DJP** capacitor with negative polarization shows a low-resistance state (LRS) under negative bias sweep 1. However, the negatively polarized domains in **DJP** start to reverse to positive polarization when the positive bias (+10 V, sweep 2) is larger than the coercive voltage. A significant current drop was observed from +10 to +15 V, which means the device goes into the high-resistance state (HRS). The device stays at HRS as the external bias is decreased to 0 V, at this stage the polarization direction is parallel with the external electric field (sweep 3). When a negative bias (−10 V, sweep 4) is applied to the device, the positively polarized domains were turned to negative polarization, such that the device is switched to LRS. The coercive voltage is ±10 V (voltages at the current peaks), corresponding to a coercive field of about 0.4 kV/cm, which is

DOI: 10.1021/jacs.9b07776
J. Am. Chem. Soc. 2019, 141, 15972−15976

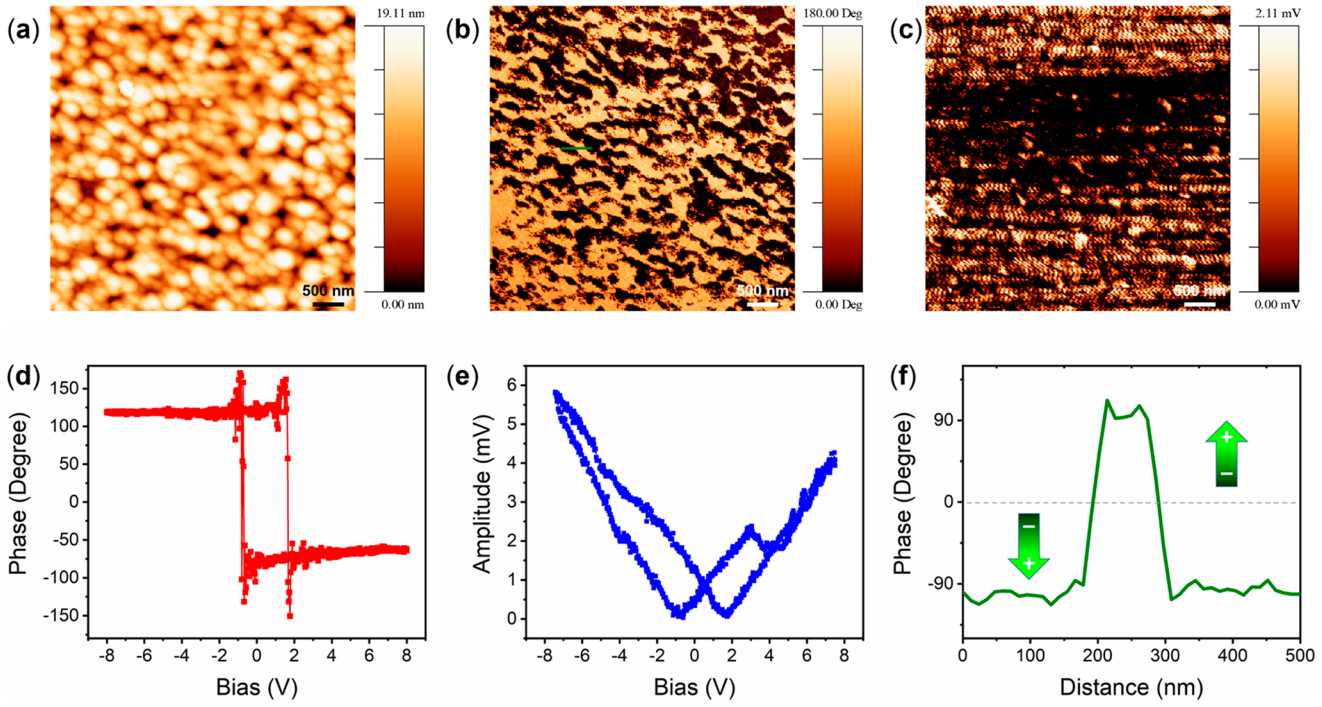

Figure 4. Piezoresponse force microscopy (PFM) for the thin-film of **DJP**. (a) Topography. (b) Out-of-plane phase. (c) Out-of-plane amplitude. (d) Phase hysteresis loop. (e) Amplitude butterfly loop. (f) Phase profile from the green line in panel b.

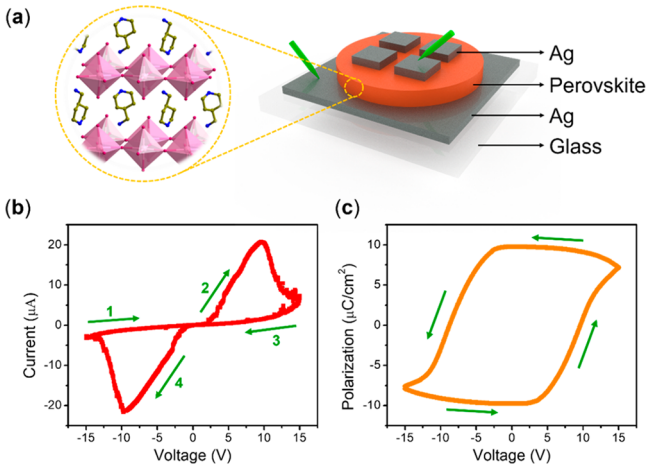

Figure 5. Electrical behavior of **DJP**. (a) Device structure. (b) I–V curve. (c) P–V curve.

comparable to that of conventional ferroelectrics such as perovskite oxides.[25]

The polarization–voltage (P–V) hysteresis loop can be obtained by integrating current over time using following eq 1:

$$P(V) = \frac{1}{AV_{\text{sweep}}} \int I \, dV \tag{1}$$

where the A is area of the capacitor and the V_{sweep} is voltage sweep rate.[26] **DJP** has a close saturated polarization (Ps) value of 9.8 μC/cm^2 at room temperature (Figure 5c). This value is larger than those of other ferroelectric RP perovskites such as $(BA)_2(MA)Pb_2Br_7$ of 3.6 μC/cm^2, $(BA)_2(MA)_2Pb_3Br_{10}$ of 2.9 μC/cm^2.[11,12]

To quantify the Rashba splitting energy of **DJP**, we applied a model that correlates the three factors which affect the experimentally observable, circularly polarized emission: Rashba parabolic band splitting k_R, hot carrier cooling rate k_{cool} and spin-flip rate k_{flip}. The circular polarization of the emission is related to the cooling rate and spin-flip rate by:

$$P = e^{-k_{\text{flip}}t_{\text{cool}}} \tag{2}$$

where P stands for degree of circular polarization of PL. The degree of circular polarization of PL has already been defined as

$$P = \left| \frac{I(\sigma_+) - I(\sigma_-)}{I(\sigma_+) + I(\sigma_-)} \right| \tag{3}$$

where $I(\sigma_+)$ and $I(\sigma_-)$ represent left and right circularly polarized PL intensity under the same circularly polarized excitation.[27] Circularly polarized excitation and PL detection is widely used to evidence the formation of spin splitting bands.[28] The presence of Rashba splitting gives rise to spin-split bands with opposite optical helicity; thus, under excitation by light of a particular polarization, the intensity of left and right circularly polarized PL will be different (Figure 6a). The sample is photoexcited by using circularly polarized 473 nm continuous wave laser, and the PL emitted is analyzed by a polarization-resolved detector (see the SI for details). As a control, a typical RP perovskite $(PEA)_2PbI_4$ was measured at room temperature (Figure S12). As expected of a centrosymmetric crystal, no difference between left and right circular-polarized emissions was observed at room temperature. As shown in Figure 6b, blue and red curve represents right and left circular polarized PL respectively under left circularly polarized excitation at 293 K. Similarly, in Figure 6c, spin flips can be observed when the source is switched to right circularly polarized excitation. The peak intensity difference indicates the existence of Rashba band splitting. The calculated circular polarization P of 24% ± 2% is then applied to eq 2 to estimate the Rashba splitting. By taking the spin-flip rate in 2D perovskites $k_{\text{flip}} \approx 4$ ps^{-1} into account,[29] the hot carrier cooling time (t_{cool}) of 0.36 ps can be estimated from eq 2. According to eq 4

DOI: 10.1021/jacs.9b07776
J. Am. Chem. Soc. 2019, 141, 15972–15976

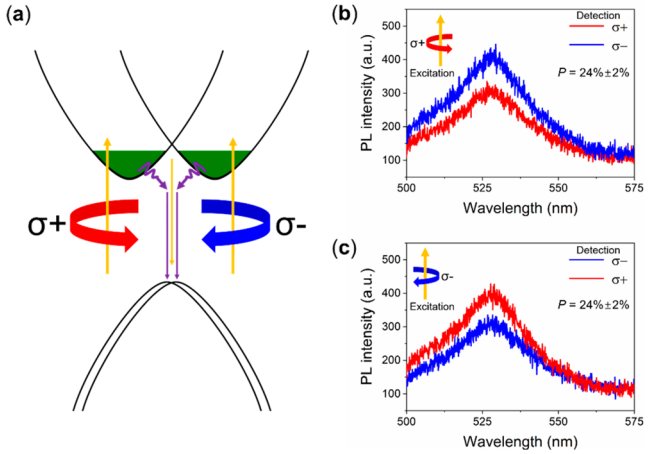

Figure 6. Rashba effect in **DJP** at 293 K. (a) Schematic illustration of spin splitting valley. (b) Left and right circularly polarized PL under left circularly polarized excitation at 473 nm. (c) Left and right circularly polarized PL under right circularly polarized excitation at 473 nm.

$$t_{cool} = \frac{(E_X - E_R)}{k_{cool}} \quad (4)$$

and taking hot carrier energy loss rate (k_{cool}) in perovskites to be ~0.1 eV/ps[30,31] (where E_X stands for excess electron energy above bandgap and E_R represents the Rashba energy barrier), we estimated a giant Rashba splitting energy E_R of 85 meV in **DJP** at 293 K. From the obtained E_R, assuming effective mass m^* = ~0.2m_0 (where m_0 is the bare electron mass),[32,33] we estimated the Rashba coefficient α to be 2.6 eV Å, based on the parabolic energy dispersion function. The offset k_R of the spin valley from the center was also estimated to be 0.067 Å^{-1} via $k_R = 2E_R/\alpha$.

CONCLUSION

In conclusion, we have demonstrated ferroelectricity and Rashba effect in a two-dimensional DJP with formula (AMP)-PbI_4 (where AMP is 4-(aminomethyl)piperidinium). A saturated polarization, P_s, value of ~9.8 μC/cm^2 with Curie temperature T_c = 352 K was measured. The P_s is higher than the conventional hybrid organic−inorganic perovskite.[11,12] A large Rashba splitting energy of 85 meV and Rashba coefficient of 2.6 eV Å was also observed. Thus, **DJP** is a room temperature Rashba ferroelectric and is a potentially useful material for spintronics. The presence of robust room temperature ferroelectricity suggests enhanced performance in photovoltaics and spintronics applications.

ASSOCIATED CONTENT

Supporting Information

The Supporting Information is available free of charge on the ACS Publications website at DOI: 10.1021/jacs.9b07776.

Experimental details, crystal structures, PXRD, PL, UV, SHG signal, PFM image, I−V curve, circularly polarized PL (PDF)

CCDC 1939808 (CIF)

CCDC 1939809 (CIF)

AUTHOR INFORMATION

Corresponding Authors

*E-mail: tzechien@ntu.edu.sg.

*E-mail: chmlohkp@nus.edu.sg.

ORCID

In-Hyeok Park: 0000-0003-1371-6641

Qiannan Zhang: 0000-0002-8139-6160

Ki Chang Kwon: 0000-0002-4004-5372

Ziyu Zhu: 0000-0001-9024-8285

Wei Yu: 0000-0003-3468-3439

Kai Leng: 0000-0003-3408-5033

David Giovanni: 0000-0002-2764-5613

Hwa Seob Choi: 0000-0003-2964-761X

Ibrahim Abdelwahab: 0000-0002-0107-5827

Qing-Hua Xu: 0000-0002-4153-0767

Tze Chien Sum: 0000-0003-4049-2719

Kian Ping Loh: 0000-0002-1491-743X

Notes

The authors declare no competing financial interest.

ACKNOWLEDGMENTS

This work was supported by the Agency for Science and Technology, Singapore, AME-IRG funding under the project "Scalable Growth of Ultrathin Ferroelectric Materials for Memory Technologies (A1983c0035)". I.-H.P. thanks to Overseas Postdoctoral Fellowship of Foresting Next-Generation Research Program through the National Research Foundation of South Korea (2017R1A6A3A03006579). Q.Z., D.G., and T.C.S. acknowledge the support from the Singapore Ministry of Education Tier 2 Grants MOE2015-T2-2-015, MOE2016-T2-1-034, and MOE2017-T2-1-001 and from the Singapore National Research Foundation Investigatorship Programme NRF-NRFI-2018-04.

REFERENCES

(1) Tsai, H.; Nie, W.; Blancon, J.-C.; Stoumpos, C. C.; Asadpour, R.; Harutyunyan, B.; Neukirch, A. J.; Verduzco, R.; Crochet, J. J.; Tretiak, S.; Pedesseau, L.; Even, J.; Alam, M. A.; Gupta, G.; Lou, J.; Ajayan, P. M.; Bedzyk, M. J.; Kanatzidis, M. G.; Mohite, A. D. High-efficiency two-dimensional Ruddlesden−Popper perovskite solar cells. *Nature* **2016**, *536*, 312−316.

(2) Leng, K.; Abdelwahab, I.; Verzhbitskiy, I.; Telychko, M.; Chu, L.; Fu, W.; Chi, X.; Guo, N.; Chen, Z.; Chen, Z.; Zhang, C.; Xu, Q.-H.; Lu, J.; Chhowalla, M.; Eda, G.; Loh, K. P. Molecularly thin two-dimensional hybrid perovskites with tunable optoelectronic properties due to reversible surface relaxation. *Nat. Mater.* **2018**, *17*, 908−914.

(3) Sha, T.-T.; Xiong, Y.-A.; Pan, Q.; Chen, X.-G.; Song, X.-J.; Yao, J.; Miao, S.-R.; Jing, Z.-Y.; Feng, Z.-J.; You, Y.-M.; Xiong, R.-G. Fluorinated 2D Lead Iodide Perovskite Ferroelectrics. *Adv. Mater.* **2019**, *0*, 1901843.

(4) Paillard, C.; Bai, X.; Infante, I. C.; Guennou, M.; Geneste, G.; Alexe, M.; Kreisel, J.; Dkhil, B. Photovoltaics with Ferroelectrics: Current Status and Beyond. *Adv. Mater.* **2016**, *28*, 5153−5168.

(5) Zhang, Q.; Solanki, A.; Parida, K.; Giovanni, D.; Li, M.; Jansen, T. L. C.; Pshenichnikov, M. S.; Sum, T. C. Tunable Ferroelectricity in Ruddlesden−Popper Halide Perovskites. *ACS Appl. Mater. Interfaces* **2019**, *11*, 13523−13532.

(6) Chen, B.; Shi, J.; Zheng, X.; Zhou, Y.; Zhu, K.; Priya, S. Ferroelectric solar cells based on inorganic−organic hybrid perovskites. *J. Mater. Chem. A* **2015**, *3*, 7699−7705.

(7) Kutes, Y.; Ye, L.; Zhou, Y.; Pang, S.; Huey, B. D.; Padture, N. P. Direct Observation of Ferroelectric Domains in Solution-Processed $CH_3NH_3PbI_3$ Perovskite Thin Films. *J. Phys. Chem. Lett.* **2014**, *5*, 3335−3339.

(8) Ye, H.-Y.; Liao, W.-Q.; Hu, C.-L.; Zhang, Y.; You, Y.-M.; Mao, J.-G.; Li, P.-F.; Xiong, R.-G. Bandgap Engineering of Lead-Halide Perovskite-Type Ferroelectrics. *Adv. Mater.* **2016**, *28*, 2579−2586.

(9) Wu, Z.; Ji, C.; Li, L.; Kong, J.; Sun, Z.; Zhao, S.; Wang, S.; Hong, M.; Luo, J. Alloying *n*-Butylamine into $CsPbBr_3$ To Give a Two-Dimensional Bilayered Perovskite Ferroelectric Material. *Angew. Chem., Int. Ed.* **2018**, *57*, 8140−8143.
(10) Liao, W.-Q.; Zhang, Y.; Hu, C.-L.; Mao, J.-G.; Ye, H.-Y.; Li, P.-F.; Huang, S. D.; Xiong, R.-G. A lead-halide perovskite molecular ferroelectric semiconductor. *Nat. Commun.* **2015**, *6*, 7338.
(11) Li, L.; Sun, Z.; Wang, P.; Hu, W.; Wang, S.; Ji, C.; Hong, M.; Luo, J. Tailored Engineering of an Unusual $(C_4H_9NH_3)_2(CH_3NH_3)_2Pb_3Br_{10}$ Two-Dimensional Multilayered Perovskite Ferroelectric for a High-Performance Photodetector. *Angew. Chem., Int. Ed.* **2017**, *56*, 12150−12154.
(12) Li, L.; Liu, X.; Li, Y.; Xu, Z.; Wu, Z.; Han, S.; Tao, K.; Hong, M.; Luo, J.; Sun, Z. Two-Dimensional Hybrid Perovskite-Type Ferroelectric for Highly Polarization-Sensitive Shortwave Photodetection. *J. Am. Chem. Soc.* **2019**, *141*, 2623−2629.
(13) Shi, P.-P.; Tang, Y.-Y.; Li, P.-F.; Liao, W.-Q.; Wang, Z.-X.; Ye, Q.; Xiong, R.-G. Symmetry breaking in molecular ferroelectrics. *Chem. Soc. Rev.* **2016**, *45*, 3811−3827.
(14) Yang, C.-K.; Chen, W.-N.; Ding, Y.-T.; Wang, J.; Rao, Y.; Liao, W.-Q.; Tang, Y.-Y.; Li, P.-F.; Wang, Z.-X.; Xiong, R.-G. The First 2D Homochiral Lead Iodide Perovskite Ferroelectrics: [R- and S-1-(4-Chlorophenyl)ethylammonium]$_2PbI_4$. *Adv. Mater.* **2019**, *31*, 1808088.
(15) Di Sante, D.; Barone, P.; Bertacco, R.; Picozzi, S. Electric Control of the Giant Rashba Effect in Bulk GeTe. *Adv. Mater.* **2013**, *25*, 509−513.
(16) Krempaský, J.; Muff, S.; Bisti, F.; Fanciulli, M.; Volfová, H.; Weber, A. P.; Pilet, N.; Warnicke, P.; Ebert, H.; Braun, J.; Bertran, F.; Volobuev, V. V.; Minár, J.; Springholz, G.; Dil, J. H.; Strocov, V. N. Entanglement and manipulation of the magnetic and spin−orbit order in multiferroic Rashba semiconductors. *Nat. Commun.* **2016**, *7*, 13071.
(17) Meng, Y.-H.; Bai, W.; Gao, H.; Gong, S.-J.; Wang, J.-Q.; Duan, C.-G.; Chu, J.-H. Ferroelectric control of Rashba spin orbit coupling at the GeTe(111)/InP(111) interface. *Nanoscale* **2017**, *9*, 17957−17962.
(18) Rinaldi, C.; Varotto, S.; Asa, M.; Sławińska, J.; Fujii, J.; Vinai, G.; Cecchi, S.; Di Sante, D.; Calarco, R.; Vobornik, I.; Panaccione, G.; Picozzi, S.; Bertacco, R. Ferroelectric Control of the Spin Texture in GeTe. *Nano Lett.* **2018**, *18*, 2751−2758.
(19) Zhai, Y.; Baniya, S.; Zhang, C.; Li, J.; Haney, P.; Sheng, C.-X.; Ehrenfreund, E.; Vardeny, Z. V. Giant Rashba splitting in 2D organic-inorganic halide perovskites measured by transient spectroscopies. *Sci. Adv.* **2017**, *3*, No. e1700704.
(20) Xia, J.; Ge, W.; Chang, K. *Semiconductor Spintronics*; World Scientific: Singapore, 2012; p 552.
(21) Mosconi, E.; Etienne, T.; De Angelis, F. Rashba Band Splitting in Organohalide Lead Perovskites: Bulk and Surface Effects. *J. Phys. Chem. Lett.* **2017**, *8*, 2247−2252.
(22) Mao, L.; Ke, W.; Pedesseau, L.; Wu, Y.; Katan, C.; Even, J.; Wasielewski, M. R.; Stoumpos, C. C.; Kanatzidis, M. G. Hybrid Dion−Jacobson 2D Lead Iodide Perovskites. *J. Am. Chem. Soc.* **2018**, *140*, 3775−3783.
(23) Ahmad, S.; Fu, P.; Yu, S.; Yang, Q.; Liu, X.; Wang, X.; Wang, X.; Guo, X.; Li, C. Dion-Jacobson Phase 2D Layered Perovskites for Solar Cells with Ultrahigh Stability. *Joule* **2019**, *3*, 794−806.
(24) Li, Y.; Milić, J. V.; Ummadisingu, A.; Seo, J.-Y.; Im, J.-H.; Kim, H.-S.; Liu, Y.; Dar, M. I.; Zakeeruddin, S. M.; Wang, P.; Hagfeldt, A.; Grätzel, M. Bifunctional Organic Spacers for Formamidinium-Based Hybrid Dion−Jacobson Two-Dimensional Perovskite Solar Cells. *Nano Lett.* **2019**, *19*, 150−157.
(25) Bao, Y.; Song, P.; Liu, Y.; Chen, Z.; Zhu, M.; Abdelwahab, I.; Su, J.; Fu, W.; Chi, X.; Yu, W.; Liu, W.; Zhao, X.; Xu, Q.-H.; Yang, M.; Loh, K. P. Gate-Tunable In-Plane Ferroelectricity in Few-Layer SnS. *Nano Lett.* **2019**, *19*, 5109−5117.
(26) Hu, L.; Dalgleish, S.; Matsushita, M. M.; Yoshikawa, H.; Awaga, K. Storage of an electric field for photocurrent generation in ferroelectric-functionalized organic devices. *Nat. Commun.* **2014**, *5*, 3279.
(27) Zeng, H.; Dai, J.; Yao, W.; Xiao, D.; Cui, X. Valley polarization in MoS_2 monolayers by optical pumping. *Nat. Nanotechnol.* **2012**, *7*, 490−493.
(28) Wu, B.; Yuan, H.; Xu, Q.; Steele, J. A.; Giovanni, D.; Puech, P.; Fu, J.; Ng, Y. F.; Jamaludin, N. F.; Solanki, A.; Mhaisalkar, S.; Mathews, N.; Roeffaers, M. B. J.; Grätzel, M.; Hofkens, J.; Sum, T. C. Indirect tail states formation by thermal-induced polar fluctuations in halide perovskites. *Nat. Commun.* **2019**, *10*, 484.
(29) Giovanni, D.; Chong, W. K.; Liu, Y. Y. F.; Dewi, H. A.; Yin, T.; Lekina, Y.; Shen, Z. X.; Mathews, N.; Gan, C. K.; Sum, T. C. Coherent Spin and Quasiparticle Dynamics in Solution-Processed Layered 2D Lead Halide Perovskites. *Adv. Sci.* **2018**, *5*, 1800664.
(30) Li, M.; Bhaumik, S.; Goh, T. W.; Kumar, M. S.; Yantara, N.; Grätzel, M.; Mhaisalkar, S.; Mathews, N.; Sum, T. C. Slow cooling and highly efficient extraction of hot carriers in colloidal perovskite nanocrystals. *Nat. Commun.* **2017**, *8*, 14350.
(31) Li, Y.; Lai, R.; Luo, X.; Liu, X.; Ding, T.; Lu, X.; Wu, K. On the absence of a phonon bottleneck in strongly confined CsPbBr3 perovskite nanocrystals. *Chem. Sci.* **2019**, *10*, 5983−5989.
(32) Yu, Z. G. Effective-mass model and magneto-optical properties in hybrid perovskites. *Sci. Rep.* **2016**, *6*, 28576.
(33) Hong, X.; Ishihara, T.; Nurmikko, A. V. Dielectric confinement effect on excitons in PbI_4-based layered semiconductors. *Phys. Rev. B: Condens. Matter Mater. Phys.* **1992**, *45*, 6961−6964.

DOI: 10.1021/jacs.9b07776
J. Am. Chem. Soc. 2019, 141, 15972−15976